Journal of Electrical and Computer Engineering Innovations
(JECEI)
Journal homepage: http://www.jecei.sru.ac.ir

Research paper

# Modeling and Analysis of Flat Double-Sided Linear Permanent Magnet Synchronous Generator by Magnetic Equivalent Circuit

***S. Niknafs[1], A. Shiri[2,*], S. Bagheri[1]***

[1]*Department of Electrical Engineering, Arak Branch, Islamic Azad University, Arak, Iran.*

[2]*Power Engineering Department, Faculty of Electrical Engineering, Shahid Rajaee Teacher Training University, Tehran, Iran.*

## Article Info

### Article History:

Received 13 January 2021
Reviewed 15 February 2021
Revised 26 March 2021
Accepted 01 April 2021

### Keywords:

Linear permanent magnet synchronous generator
Flat double-sided structure
Magnetic equivalent circuit
Finite element method

[*]Corresponding Author's Email Address:
*abbas.shiri@sru.ac.ir*

## Abstract

**Background and Objectives:** In recent years, linear generators have been broadly utilized to harness wave motion energy. There are various types of linear generators with different magnetic and geometric structures. Among these generators, linear permanent magnet synchronous generator provides a higher energy density than other generators. Due to the simplicity of the structure and the low cost of producing a flat double-sided structure, this type of structure is investigated in this paper.

**Methods:** The purpose of the paper can be divided into two main sections: first, modeling of the flat double-sided linear permanent magnet synchronous generator by using magnetic equivalent circuit (MEC) method and second, deriving the generator electrical equations which are used in analysis and design process.

**Results:** The behavior of the linear permanent magnet synchronous generator is studied and the induced voltages are calculated. The no-load and loaded conditions of the generator with different loads are investigated and the voltage and the current of the load are obtained.

**Conclusion:** In order to confirm the results, finite element method (FEM) is employed. The designed linear generator is simulated by FEM. Comparing the results obtained by MEC and FEM show good agreements between two methods, validating the presented modelling method.

©2022 JECEI. All rights reserved.

## Introduction

With ever-increasing environmental concerns, a considerable attempt has been made to develop renewable energy sources (RESs). Among these sources, ocean wave energy is a major source for generating electricity [1], [2]. It has the highest energy density and availability and is also more predictable than other renewable energies [3]-[10]. This topic has been extensively studied and several systems have been developed to exploit wave power [11]. A suitable system for harnessing wave energy is a wave energy converter that is used to convert wave energy into electrical energy [12]-[15]. The wave energy is transferred to the buoy of the wave energy converter, where it is converted into kinetic energy, and finally it is extracted as electrical energy [16], [17]. In recent years, linear generators have been widely utilized in these converters [18]. So, their modeling is one of the most important issues in the design and analysis of these generators. There are different modelling methods; one of them is magnetic equivalent circuit (MEC) modeling, the main purpose of which is to determine the magnet or coil flux density at different points of the generator. Hence, the MEC method has been continuously

improved and now enjoys many capabilities [19]. This is an effective method in modeling the flux density distribution in permanent magnet (PM) machines and can consider the effect of saturation [20]-[23]. The MEC is extensively used for the analysis and design of electrical machinery [24]. For example, a 3D MEC method has been proposed in [25] to analyze the coupling flux characteristics and electromagnetic force of a double-sided linear switched reluctance machine (LSRM). Then, flux linkage curves calculated by MEC are compared with the 3D results of FEM and the empirical results. Reference [26] compares the nodal and mesh-based MEC formulations of a magnetic system. The Newton-Raphson algorithm is used to solve the algebraic system and draw conclusions about the computational efficiency of the two formulae in linear and nonlinear cases. The two formulations perform similarly in linear conditions; however, in nonlinear conditions, the mesh-based model performs significantly superior to the nodal-based formulation. A quasi-3D nonlinear MEC model is proposed for double-sided axial flux PM machines with concentrated coils [27]. The model can take into account not only the effect of local magnetic saturation but also the 3D flux distribution. To evaluate the reliability of the MEC model, two prototypes of this machine have been considered, and by comparing the calculated parameters of the MEC model with FEM and experimental results, its validity has been confirmed. According to performed research on the LPMSGs, the magnetic equivalent circuit (MEC) model of flat double-sided LPMSGs has not yet been investigated in literature. Therefore, in this paper, the MEC model is proposed for this type of generator. Then, by using this model, the performance of the machine is investigated at no-load and loaded conditions. The second section of the present paper describes the modeling of LPMSG using the MEC method. The electrical equations of the system are provided in the third section. Eventually, the simulation results and the validation are presented in the fourth and fifth sections, respectively.

## Generator Modeling Using The MEC Method

In this section, MEC method is proposed for modelling an air-cored flat double-sided LPMSG. There are different topologies for these generators [28], [29]: one with integrated back-iron [28] and the other with C core module type [29]. In generators with integrated iron, the normal force acting on both sides of the generator is very high; however, in C core module type, the normal force between two modules in both sides reduces due to separated modules. In this paper, flat module type configuration is considered to decrease the normal force. The 2D model of the mentioned configuration is depicted in Fig. 1. In this figure, each translator module is composed of a magnet and the iron.

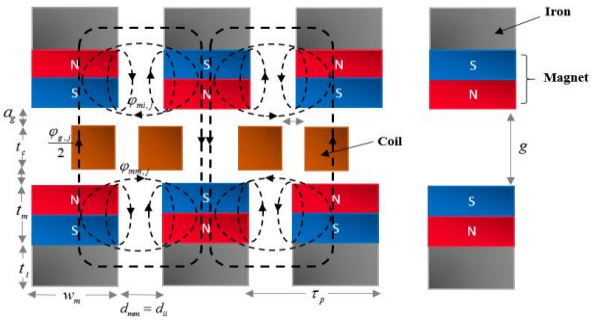


Fig. 1: 2D model of the flat double-sided LPMSG.

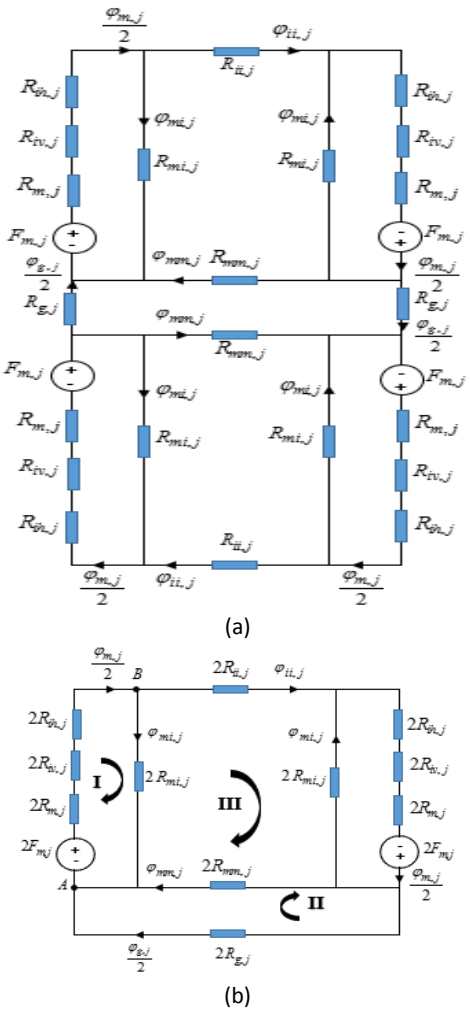


Fig. 2: The proposed MEC model of the j$^{th}$ path for a pole; (a) general layout and (b) summarized layout.

It should be mentioned that to decrease the leakage fluxes and increase the performance of the generator, the distance between two adjacent modules should be as low as possible. In Fig. 1 $t_i$ , $t_m$ , and $t_c$ denote the thickness of the iron, the thickness of the magnet, and the thickness of the coil, respectively. Also, $\tau_p$ is the pole pitch, $W_m$ is the width of the magnet, and $a_g$ is the air gap between the magnet and the coil. Moreover,

$d_{mm}$ and $d_{ii}$ represent the distance between two adjacent magnets and the distance between two adjacent irons, respectively. Based on the flux paths in Fig. 1 and considering the model symmetry, the proposed MEC model of the j[th] path for a pole is shown in Fig. 2. In Fig. 2, $R_{m,j}$, $R_{iv,j}$, and $R_{ih,j}$ are the PM, iron vertical section, and iron horizontal section reluctances for the j[th] path, respectively, and are obtained from the following equations:

$$R_{m,j} = \frac{t_m}{w_m l_a \mu_0 \mu_m} \quad (1)$$

$$R_{iv,j} = \frac{(\frac{t_i}{2})}{w_m l_a \mu_0 \mu_i} \quad (2)$$

$$R_{ih,j} = \frac{(\frac{w_m}{2})}{t_i l_a \mu_0 \mu_i} \quad (3)$$

where, $l_a$ is the active length of the generator, $\mu_o$ is the relative permeability of the air, $\mu_m$ is the relative permeability of the magnet, and $\mu_i$ is the relative permeability of the iron. Also, g shows the air gap and $R_{g,j}$ is the reluctance of the air gap between the PMs above and below the j[th] path, given as follows:

$$g = 2a_g + t_c \quad (4)$$

$$R_{g,j} = \frac{g}{w_m l_a \mu_0} \quad (5)$$

On the other hand, $R_{mi,j}$ represents the reluctance of the leakage flux path of the magnet to the iron and $R_{mm,j}$ indicates the reluctance of the leakage flux path between two adjacent PMs in the j[th] path, which are obtained from the following equations, respectively:

$$R_{mi,j} = \frac{t_m + t_i}{w_m l_a \mu_0} \quad (6)$$

$$R_{mm,j} = \frac{\tau_p}{(\frac{t_c}{2} + a_g) l_a \mu_0} \quad (7)$$

In the above equation, $\tau_p$ is the pole pitch which is obtained by the following equation [28]:

$$\tau_p = \beta \frac{l_w}{N_c} \quad (8)$$

where $\beta$ is a constant with a value of less than one, $l_w$ is the length of the working section, and $N_c$ is the number of coils. Also, $R_{ii,j}$ is the leakage flux path reluctance between two adjacent irons of the j[th] path, which is obtained from the following equation:

$$R_{ii,j} = \frac{d_{ii}}{t_i l_a \mu_0} \quad (9)$$

According to Fig. 2, $\varphi_{m,j}$, $\varphi_{g,j}$, $\varphi_{mi,j}$, $\varphi_{mm,j}$, and $\varphi_{ii,j}$ represent the magnet flux, air gap flux, magnet-to-iron leakage flux, magnet-to-magnet leakage flux, and iron-to-iron leakage flux, respectively.

Eventually, after obtaining the reluctances of the flux paths and applying KVL law to the three closed paths I, II, and III and KCL law to nodes A and B in Fig. 2 (b), the fluxes are calculated using the following matrix:

$$\begin{bmatrix} \varphi_{m,j} \\ \varphi_{g,j} \\ \varphi_{mi,j} \\ \varphi_{mm,j} \\ \varphi_{ii,j} \end{bmatrix} = \begin{bmatrix} R_{m,j}+R_{iv,j}+R_{ih,j} & 0 & 2R_{mi,j} & 0 & 0 \\ 0 & R_{g,j} & 0 & -2R_{mm,j} & 0 \\ 0 & 0 & -4R_{mi,j} & 2R_{mm,j} & 2R_{ii,j} \\ -0.5 & 0.5 & 1 & 1 & 0 \\ 0.5 & 0 & -1 & 0 & -1 \end{bmatrix}^{-1} \begin{bmatrix} 2F_{m,j} \\ 0 \\ 0 \\ 0 \\ 0 \end{bmatrix} \quad (10)$$

In the above equation, $F_{m,j}$ is the magnet magnetomotive force (MMF) in j[th] path, which is obtained from the following equation:

$$F_{m,j} = t_m (\frac{B_r}{\mu_0 \mu_m}) \quad (11)$$

where, $B_r$ is the magnetic residue of the magnet. The cross-section of the PM is obtained from the following equation:

$$A = w_m l_a \quad (12)$$

Therefore, the flux density of the air gap of the j[th] path $(B_{g,j})$ can be obtained using (13). The flowchart for calculating this density is shown in Fig. 3.

$$B_{g,j} = \frac{\varphi_{g,j}}{A} \quad (13)$$

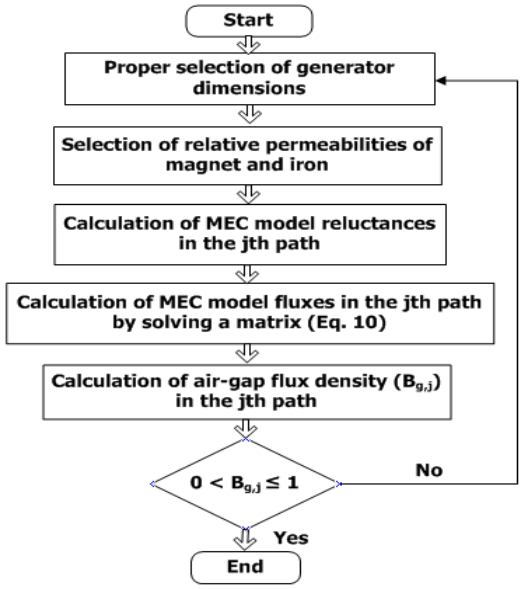


Fig. 3: The flowchart for calculating flux density of the air gap.

## Generator Electrical Equations

In this section, electrical equations for calculating the induced voltages and the load current and voltage are given. The cross-section of the wire is calculated as:

$$A_w = \frac{\pi(w_d)^2}{4} \quad (14)$$

In the above equation, $w_d$ is the diameter of the wire. Also, the thickness of the coil $(t_c)$ can be obtained as follows:

$$t_c = \frac{N_t A_w}{w_a K_f} \quad (15)$$

where, $N_t$ is the number of turns of each coil and $K_f$ is the fill factor. $w_a$ shows the average outer width $(w_o)$ and inner width $(w_i)$ of the coil, which are expressed as follows [30]:

$$w_a = \frac{w_o + w_i}{2} \quad (16)$$

$V_t$ and $V_c$ represent the peak voltages of the EMF of each coil turn and each coil, respectively [31]:

$$V_t = 2B_g l_a v_l \quad (17)$$

$$V_c = N_t K_p K_s V_t \eta_e \quad (18)$$

In the above equations, $v_l$ is the maximum linear speed and $\eta_e$ is the end-effect factor. Given that N is the number of coils in each phase, the EMF voltage of each phase $(V_p)$ is defined as follows:

$$V_p = NV_c \quad (19)$$

To obtain the load current, it is necessary to calculate the total impedance of each phase $(Z_p)$, which is obtained from the following equation:

$$Z_p = R_l + R_c + jX_c \quad (20)$$

In (20), $R_l$ is the load resistance of the generator in the loaded case, $X_c$ is the coil reactance, and $R_c$ is the coil resistance which is derived as follows:

$$R_c = N_t R_w M_l \quad (21)$$

where, $R_w$ is the resistance of the wire, and $M_l$ is the average length per turn, which is expressed by the following equation:

$$M_l = 2l_a + (\pi w_a) \quad (22)$$

Finally, $I_l$ and $V_l$ are the load current and voltage, which are calculated from the following equations:

$$I_l = \frac{V_p}{Z_p} \quad (23)$$

$$V_l = R_l I_l \quad (24)$$

## MEC Simulation Results and Discussion

The values of the generator parameters under study are tabulated in Table 1. In this table, the distance between two adjacent irons is chosen 8 mm which is high value for practical applications. As mentioned before, to decrease the leakage fluxes, this value should be chosen as lower as possible. The generator is considered in the no-load and loaded conditions with different loads. In this section, simulations are performed using MEC, where the maximum linear speed is $v_l = 1m/s$.

In this simulation, the peak induced phase voltage is 203 V, and the voltage and current values in the loaded case are given in Table 2. Fig. 4 shows the magnetic field intensity in terms of the relative permeability of the magnet. Relative permeability decreases with increasing field intensity.

## Validation by FEM

To confirm the proposed method based on MEC, the simulations of the generator in the no-load and loaded conditions were carried out by FEM. Fig. 5 illustrates the peak induced phase voltage in the loaded case of the generator, which is 202.3 V.

Table 1: The parameters of the studied generator

| Parameter | Symbol | Value | Parameter | Symbol | Value |
|---|---|---|---|---|---|
| active length (m) | $l_a$ | 0.2 | magnet width (mm) | $w_m$ | 44 |
| working section length (m) | $l_w$ | 0.94 | coil thickness (mm) | $t_c$ | 16 |
| pole pitch (mm) | $\tau_p$ | 52 | iron thickness (mm) | $t_i$ | 10 |
| magnet thickness (mm) | $t_m$ | 10 | space between coils (mm) | $s_c$ | 2.2 |
| air gap between magnet and coils (mm) | $a_g$ | 3 | distance between two adjacent irons (mm) | $d_{ii}$ | 8 |
| magnetic residue of the magnets (T) | $B_r$ | 1.2 | number of coils | $N_c$ | 15 |
| number of active poles each side | $N_a$ | 18 | wire thickness (mm) | $w_d$ | 0.9 |
| coil outer width (mm) | $w_o$ | 64 | coil inner width (mm) | $w_i$ | 30 |
| pitch factor (Rad) | $K_p$ | 0.99 | fill factor | $K_f$ | 0.645 |
| distance between two adjacent magnets (mm) | $d_{mm}$ | 8 | spread factor (Rad) | $K_s$ | 0.96 |
| coil turns | $N_t$ | 276 | end-effect factor | $\eta_e$ | 0.945 |

Table 2: MEC simulation results in different loads

| Load [Ω] | 10 | 20 | 50 | 100 |
|---|---|---|---|---|
| Load voltage [V] | 56.1 | 87.85 | 133.18 | 160.8 |
| Load current [A] | 5.61 | 4.39 | 2.66 | 1.61 |

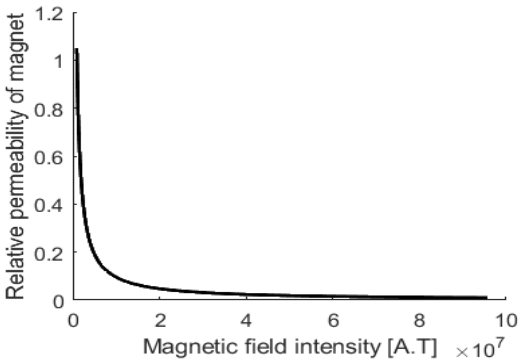


Fig. 4: The magnetic field intensity in terms of relative permeability of the magnet.

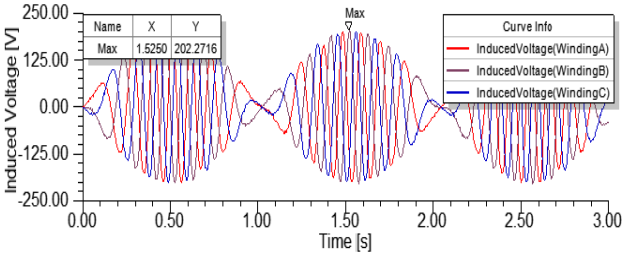


Fig. 5: Induced voltage in no load.

In under load condition, different loads are considered and the voltage and current values for each load obtained by FEM. To make better comparison, the results obtained by MEC are compared with the results of the FEM, in Table 3. As it is seen from the table, the load voltages and currents obtained by the two methods are close enough to each other, confirming the proposed MEC method.

Table 3: The comparison of the MEC and FEM results with different loads

| Load [Ω] | Load voltage [V] | | | Load current [A] | | |
|---|---|---|---|---|---|---|
| | MEC | FEM | Error [%] | MEC | FEM | Error [%] |
| 10 | 56.1 | 61.7 | 9.10 | 5.61 | 5.92 | 5.24 |
| 20 | 87.85 | 95.3 | 7.81 | 4.39 | 4.76 | 7.77 |
| 50 | 133.18 | 140 | 4.87 | 2.66 | 2.8 | 5.00 |
| 100 | 160.8 | 165.9 | 3.07 | 1.61 | 1.66 | 3.01 |

Figs. 6 and 7 show the induced voltage and current, respectively, where the peak voltage is 200.6 V and the peak current is 2.8 A. According to the results, the peak induced phase voltage in the no-load case is 1.7 V, which is higher than the peak induced voltage in the loading case with a load of 50 Ω.

Fig. 8 shows the generator flux density distribution with a maximum density of 1.3 T. Flux lines in different parts of the generator are shown in Fig. 9. The leakage fluxes are obvious in the figure, due to high value of the distance between two adjacent irons (8 mm).

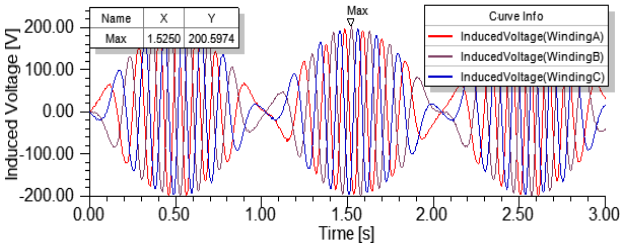


Fig. 6: Induced voltage in loaded.

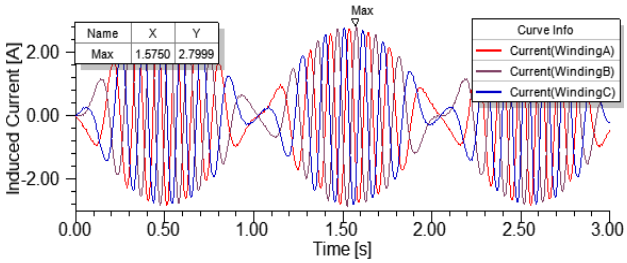


Fig. 7: Induced current in loaded.

## Conclusion

In this paper, the MEC model of a flat double-sided LPMSG is proposed. Additionally, the fluxes are calculated for the closed $j^{th}$ path, and the flux density of the air gap in this path is obtained. Electrical equations are expressed to obtain the voltage and current of the generator load, and the results of the proposed MEC model are validated by FEM in Maxwell software to demonstrate the effectiveness of the method.

## Author Contributions

This paper is the result of S. Niknafs's Ph.D. project which is supervised and advised by A. Shiri and S. Bagheri, respectively. S. Niknafs did the simulations and wrote the manuscript. S. Niknafs and A. Shiri presented the MEC model for this type of generator A. Shiri interpreted the results and edited the manuscript. S. Bagheri reviewed the manuscript.

## Acknowledgment

The authors would like to thank the anonymous reviewers and the editors of JECEI for their valuable

comments and suggestions for improving quality of the paper.

## Conflict of Interest

The authors declare no potential conflict of interest regarding the publication of this work. In addition, the ethical issues including plagiarism, informed consent, misconduct, data fabrication and, or falsification, double publication and, or submission, and redundancy have been completely witnessed by the authors.

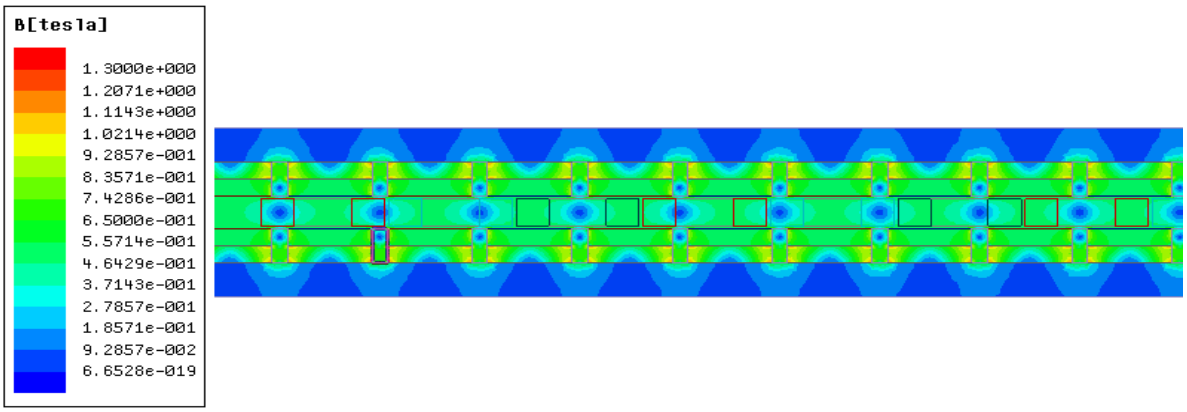


Fig. 8: Flux density distribution in the generator.

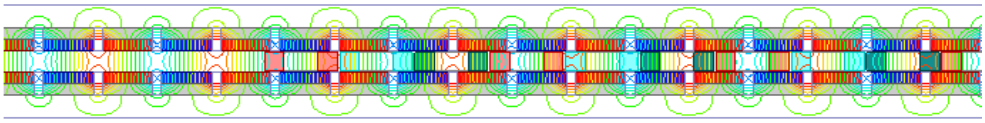

Fig. 9: Flux lines in different parts of the generator.

## Abbreviations

| | |
|---|---|
| $a_g$ | air gap between magnet and coils |
| $B_r$ | magnetic residue of the magnets |
| $d_{ii}$ | distance between two adjacent irons |
| $d_{mm}$ | distance between two adjacent magnets |
| $K_p$ | pitch factor |
| $l_a$ | active length |
| $l_w$ | working section length |
| $M_l$ | the average length per turn |
| $N_a$ | number of active poles each side |
| $N_c$ | number of coils |
| $N_t$ | coil turns |
| $s_c$ | space between coils |
| $t_c$ | coil thickness |
| $t_i$ | iron thickness |
| $t_m$ | magnet thickness |
| $w_d$ | wire thickness |
| $w_i$ | coil inner width |
| $w_m$ | magnet width |
| $w_o$ | coil outer width |

## References

[1] S. Molla, O. Farrok, K. M. Muttaqi, M. R. Islam, "Design of a direct drive linear generator with high flux density magnetic cores for oceanic wave energy conversion," in Proc. IEEE International Conference on Applied Superconductivity and Electromagnetic Devices (ASEMD): 1-2, 2018.

[2] S. Molla, O. Farrok, M.R. Islam, K.M. Muttaqi, "Analysis and design of a high performance linear generator with high grade magnetic cores and high temperature superconducting coils for oceanic wave energy conversion," IEEE Trans. Appl. Supercond., 29(2): 1-5, 2019.

[3] H. Jing, B. Cao, Y. Zou, M. Izumi, N. Maki, X. Chen, P. Xu, "A power take-off device with an hts synchronous reluctance linear generator," IEEE Trans. Appl. Supercond., 30(8): 1-6, 2020.

[4] O. Farrok, M.R. Islam, M.R. Sheikh, Y. Guo, J. Zhu, G. Lei, "Oceanic wave energy conversion by a novel permanent magnet linear generator capable of preventing demagnetization," IEEE Trans. Ind. Appl., 54(6): 6005-6014, 2018.

[5] H. Jing, N. Maki, T. Ida, M. Izumi, "Design study of large-scale HTS linear generators for wave energy conversion," IEEE Trans. Appl. Supercond., 27(4): 1-5, 2017.

[6] M. Johnson, M.C. Gardner, H.A. Toliyat, S. Englebretson, W. Ouyang, C. Tschida, "Design, construction, and analysis of a large-scale inner stator radial flux magnetically geared generator for wave energy conversion," IEEE Trans. Ind. Appl., 54(4): 3305-3314, 2018.

[7] O. Farrok, M.R. Islam, M.R. Sheikh, Y. Guo, J. Zhu, G. Lei, "A novel method to avoid degradation due to demagnetization of PM linear generators for oceanic wave energy extraction," in Proc. 2017 20th International Conference on Electrical Machines and Systems (ICEMS): 1-6, 2017.

[8] S. Molla, O. Farrok, A. Rahman, M.S. Bashir, M.R. Islam, A.Z. Kouzani, M.P. Mahmud, "Increase in volumetric electrical power density of a linear generator by winding optimization for wave energy extraction," IEEE Access., 8: 181605-181618, 2020.

[9] R.P. Mendes, M.R. Calado, S.J. Mariano, C.M. Cabrita, "Design of a tubular switched reluctance linear generator for wave energy conversion based on ocean wave parameters," in Proc. International Aegean Conference on Electrical Machines and Power Electronics and Electromotion: 146-151, 2011.

[10] X. Xiao, X. Huang, Q. Kang, "A hill-climbing-method-based maximum-power-point-tracking strategy for direct-drive wave energy converters," IEEE Trans. Ind. Electron., 63(1): 257-267, 2015.

[11] L. Cappelli, F. Marignetti, G. Mattiazzo, E. Giorcelli, G. Bracco, S. Carbone, C. Attaianese, "Linear tubular permanent-magnet generators for the inertial sea wave energy converter," IEEE Trans. Ind. Appl., 50(3): 1817-28, 2013.

[12] M. Jama, A. Wahyudie, "Online damping strategy for controlling heaving wave energy converters using three-phase bridge boost rectifier," IEEE Access., 5: 7682-91, 2017.

[13] J. Zhang, H. Yu, Q. Chen, M. Hu, L. Huang, Q. Liu, "Design and experimental analysis of AC linear generator with Halbach PM arrays for direct-drive wave energy conversion," IEEE Trans. Appl. Supercond., 24(3): 1-4, 2013.

[14] J. Kim, J.Y. Kim, J.B. Park, "Design and optimization of a 8kW linear generator for a direct-drive point absorber," in Proc. OCEANS-San Diego: 1-6, 2013.

[15] M.S. Bashir, O. Farrok, "Generation of electrical power by using high graded permanent magnet linear generator in wave energy conversion," in Proc. International Conference on Advances in Science, Engineering and Robotics Technology (ICASERT): 1-5, 2019.

[16] Y.J. Oh, J.S. Park, B.J. Hyon, J. Lee, "Novel control strategy of wave energy converter using linear permanent magnet synchronous generator," IEEE Trans. Appl. Supercond., 28(3): 1-5, 2018.

[17] D.T. Ba, N.D. Anh, P. Van Ngoc, "Numerical simulation and experimental analysis for a linear trigonal double-face permanent magnet generator used in direct driven wave energy conversion," Procedia Chem., 14: 130-7, 2015.

[18] L. Huang, M. Chen, L. Wang, F. Yue, R. Guo, X. Fu, "Analysis of a hybrid field-modulated linear generator for wave energy conversion," IEEE Trans. Appl. Supercond., 28(3): 1-5, 2018.

[19] B. Sheikh-Ghalavand, S. Vaez-Zadeh, A. Hassanpour Isfahani, "An improved magnetic equivalent circuit model for iron-core linear permanent-magnet synchronous motors," IEEE Trans. Magn., 46(1): 112-20, 2009.

[20] H. Hu, J. Zhao, X. Liu, Y. Guo, "Magnetic field and force calculation in linear permanent-magnet synchronous machines accounting for longitudinal end effect," IEEE Trans. Ind. Electron., 63(12): 7632-43, 2016.

[21] A. Souissi, M.W. Zouaghi, I. Abdennadher, A. Masmoudi, "MEC-based modeling and sizing of a tubular linear PM synchronous machine," IEEE Trans. Ind. Appl., 51(3): 2181-94, 2014.

[22] A. Hanic, D. Zarko, Z. Hanic, "A novel method for no-load magnetic field analysis of saturated surface permanent-magnet machines using conformal mapping and magnetic equivalent circuits," IEEE Trans. Energy Convers., 31(2): 740-9, 2015.

[23] H. Hu, J. Zhao, X. Liu, Y. Guo, J. Zhu, "No-load magnetic field and cogging force calculation in linear permanent-magnet synchronous machines with semi-closed slots," IEEE Trans. Ind. Electron., 64(7): 5564-75, 2016.

[24] H. Gorginpour, H. Oraee, R.A. McMahon, "A novel modeling approach for design studies of brushless doubly fed induction generator based on magnetic equivalent circuit," IEEE Trans. Energy Convers., 28(4): 902-912, 2013.

[25] H. Chen, X. Liu, W. Yan, "Three-Dimensional Magnetic Equivalent Circuit Research of Double-Sided Switched Reluctance Linear Machine," IEEE Trans. Appl. Supercond., 30(4): 1-8, 2020.

[26] H.W. Derbas, J.M. Williams, A.C. Koenig, S.D. Pekarek, "A comparison of nodal-and mesh-based magnetic equivalent circuit models," IEEE Trans. Energy Convers., 24(2): 388-396, 2009.

[27] W. Tong, S. Wang, S. Dai, S. Wu, R. Tang, "A quasi-three-dimensional magnetic equivalent circuit model of a double-sided axial flux permanent magnet machine considering local saturation," IEEE Trans. Energy Convers., 33(4): 2163-2173, 2018.

[28] A. Wahyudie, M. Jama, T.B. Susilo, B.F. Mon, H. Shaaref, H. Noura, "Design and testing of a laboratory scale test rig for wave energy converters using a double-sided permanent magnet linear generator," IET Renewable Power Gener., 11(7): 922-930, 2017.

[29] A.S. McDonald, M.A. Mueller, J.G. Jeffrey, "Development of a novel permanent magnet linear generator topology for direct-drive wave energy converters", in Proc. IET Conference on Power Electronics, Mechanics and Drives: 81-85, 2008.

[30] A. Wahyudie, T.B. Susilo, M. Jama, B.F. Mon, H. Shaaref, "Design of a double-sided permanent magnet linear generator for laboratory scale ocean wave energy converter," In Proc. OCEANS 2017-Anchorage: 1-5, 2017.

[31] O. Saeed, A. Wahyudie, T. B. Susilo, H. Shareef, "Simple resonance circuit to improve electrical power conversion in a two-sided planar permanent magnet linear generator for wave energy converters," IEEE Access., 5: 18654-18664, 2017.

## Biographies

**Sabiyeh Niknafs** is Ph.D. student in power engineering at Islamic Azad University, Arak Branch. Her areas of research interests include linear electric machines, electrical machine design and modeling.

**Abbas Shiri** received the B.Sc. degree from Tabriz University and M.Sc. and Ph.D. degrees from Iran University of Science and Technology all in electrical engineering in 2004, 2006 and 2013, respectively. He is currently an assistant professor at Shahid Rajaee Teacher Training University, Tehran, Iran. His areas of research interests include linear electric machines, electromagnetic systems and actuators, electrical machine design and modeling.

**Sajad Bagheri** received the Ph.D. degree in electrical engineering from Semnan University, Semnan, Iran, in 2017. He is currently an Assistant Professor with the Department of Electrical Engineering, Arak Branch, Islamic Azad University, Arak, Iran. His research interests include power system protection and the application of artificial intelligence and machine learning in it, diagnosis, condition monitoring, and detection of winding movement of power transformers. Dr. Bagheri is a member of the Young Researchers and Elite Club, the Iranian Wind Energy Association, and the Iranian Society of Smart Grid.

**Copyrights**
©2022 The author(s). This is an open access article distributed under the terms of the Creative Commons Attribution (CC BY 4.0), which permits unrestricted use, distribution, and reproduction in any medium, as long as the original authors and source are cited. No permission is required from the authors or the publishers.

**How to cite this paper:**
S. Niknafs, A. Shiri, S. Bagheri, "Modeling and analysis of flat double-sided linear permanent magnet synchronous generator by magnetic equivalent circuit," J. Electr. Comput. Eng. Innovations, 10(1): 17-24, 2022.

**DOI:** 10.22061/JECEI.2021.7782.434

**URL:** https://jecei.sru.ac.ir/article_1549.html